Cell Reports, Volume *43*

Supplemental information

Opposing tumor-cell-intrinsic and -extrinsic roles of the IRF1 transcription factor in antitumor immunity

Prabhat K. Purbey, Joowon Seo, Manash K. Paul, Keisuke S. Iwamoto, Allison E. Daly, An-Chieh Feng, Ameya S. Champhekar, Justin Langerman, Katie M. Campbell, Dörthe Schaue, William H. McBride, Steven M. Dubinett, Antoni Ribas, Stephen T. Smale, and Philip O. Scumpia

A

Chromatogram of *Irf1*$^{-/-}$ clone I1 (deletion of "A")

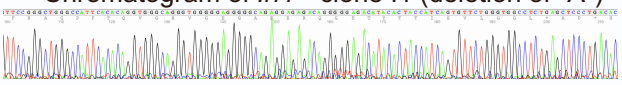

A. A seq(WT): F R S W A I H T G

Nucleotide-alignment
WT: TTCCGGAGCTGGGCCATTCACACAGG
I1: TTCCGG-GCTGGGCCATTCACACAGG
PAM

B

Chromatogram of *Irf1*$^{-/-}$ clone I3 (deletion of "TG")

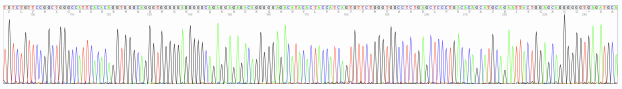

A. A seq(WT): S W A I H T G R Y

Nucleotide Alignment
WT: AGCTGGGCCATTCACACAGGTGGGCAG
I3: AGCTGGGCCATTCACACAGG--GGCAG
PAM

C

Chromatogram of *Sting*$^{-/-}$ clone S1 (deletion of "G")

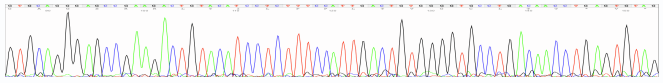

A. A seq(WT): F P L D C G V P D N L S

Nucleotide-alignment
WT: TTTCCATTGGACTGTGGGGTGCCTGACAACCTGAGT
S1: TTTCCATTG ACTGTGGGGTGCCTGACAACCTGAGT
PAM

D

Chromatogram of *Sting*$^{-/-}$ clone S3 ("T" and "TT" deletion)

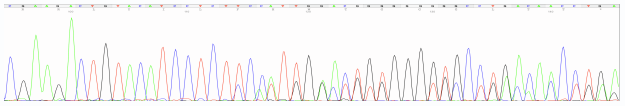

A. A seq(WT): Y I L F P L D C G V P D

Nucleotide Alignment
WT: TACATCCTCTTTCCATTGGACTGTGGGGTGCCTGAC
S3_Allele1: TACATCCTCTT-CCATTGGACTGTGGGGTGCCTGAC
S3_Allele2: TACATCCTCT--CCATTGGACTGTGGGGTGCCTGAC
PAM

E MTS Assay to monitor proliferation of WT, *Sting*$^{-/-}$ and *Irf1*$^{-/-}$ clones

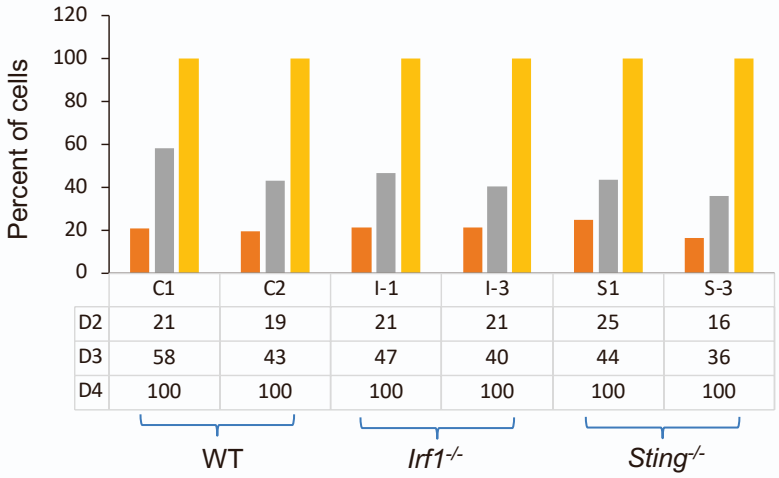

	C1	C2	I-1	I-3	S1	S-3
D2	21	19	21	21	25	16
D3	58	43	47	40	44	36
D4	100	100	100	100	100	100

F MTS Assay to monitor radiation sensitivity of WT, *Sting*$^{-/-}$ and *Irf1*$^{-/-}$ clones

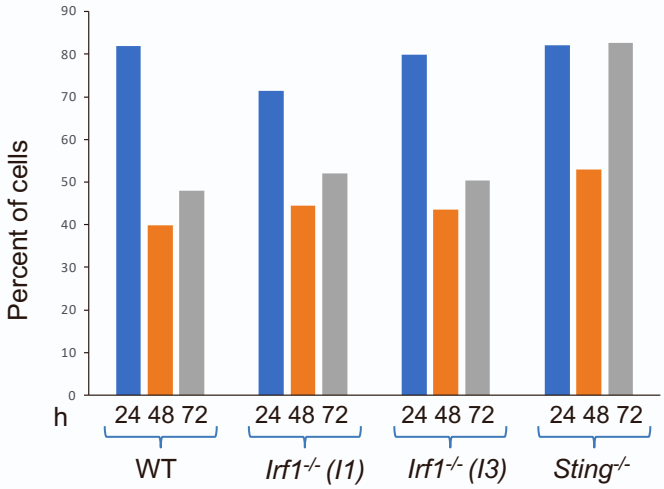

G Clonogenic Survival Assay of WT, *Sting*$^{-/-}$ and *Irf1*$^{-/-}$ clones

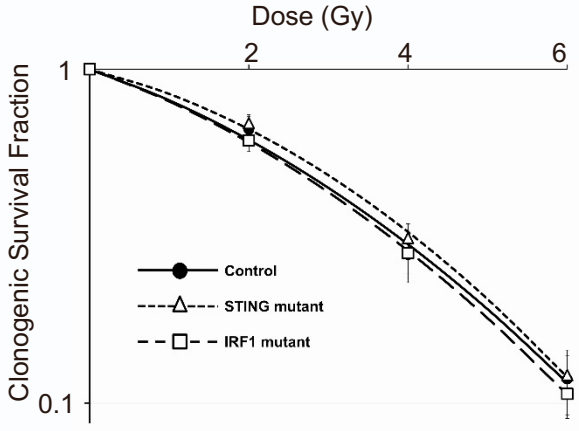

H

Tumor Cell line	Immunogenicity	TMB	Basal MHC-I level
MC38	High		
B16F10			
YUMM2.1	low		

I

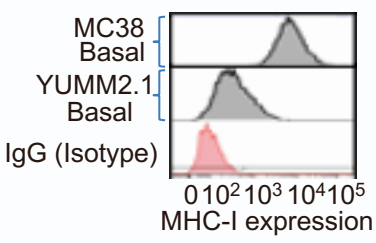

Figure S1. (Related to Figure 1) Comparable Proliferation and Radiosensitivity of WT and Mutant MC38 Clones. (A-B) Shows representative Sanger sequencing chromatogram and nucleotide alignment of IRF1 mutant MC38 clones (I1 and I3). Mutants created stop codons a few nucleotides after the mutation site that disrupts the DNA binding domain, and do not translate nuclear localization and transactivation domains of IRF1. (C-D) Shows representative Sanger sequencing chromatogram and nucleotide alignment of STING mutant MC38 clones (S1 and S3). These mutants created stop codons a few nucleotides after the mutation site that may produce truncated STING protein without the cyclic-di-GMP-binding and C terminal IRF3 activating domains. **(E)** MTS assay showing proliferation of 2 each of WT, *Irf1*$^{-/-}$ and *Sting*$^{-/-}$ clones upto day 4. **(F)** MTS assay to show radiosensitivity. Percent of surviving fractions are shown on the y axis after 24, 48 and 72h post 10Gy of x-ray exposure. **(G)** Clonogenic assay indicating comparable number of clones obtained in WT*, Irf1*$^{-/-}$ and *Sting*$^{-/-}$ on day 11 post 2, 4 and 6GY of IR. **(H)** Table representation of tumor mutation burden (TMB), immunogenicity and basal expression of MHC-I in mouse colon (MC38), and two types of melanomas (B16F10 and YUM2.1). **(I)** Shows low level surface expression of MHC-I in YUMM2.1 (middle histogram) as compared to MC38 (top histogram). The bottom histogram is the MC38 profile when stained with isotype control antibody.

In vivo Yumm2.1 tumor analysis

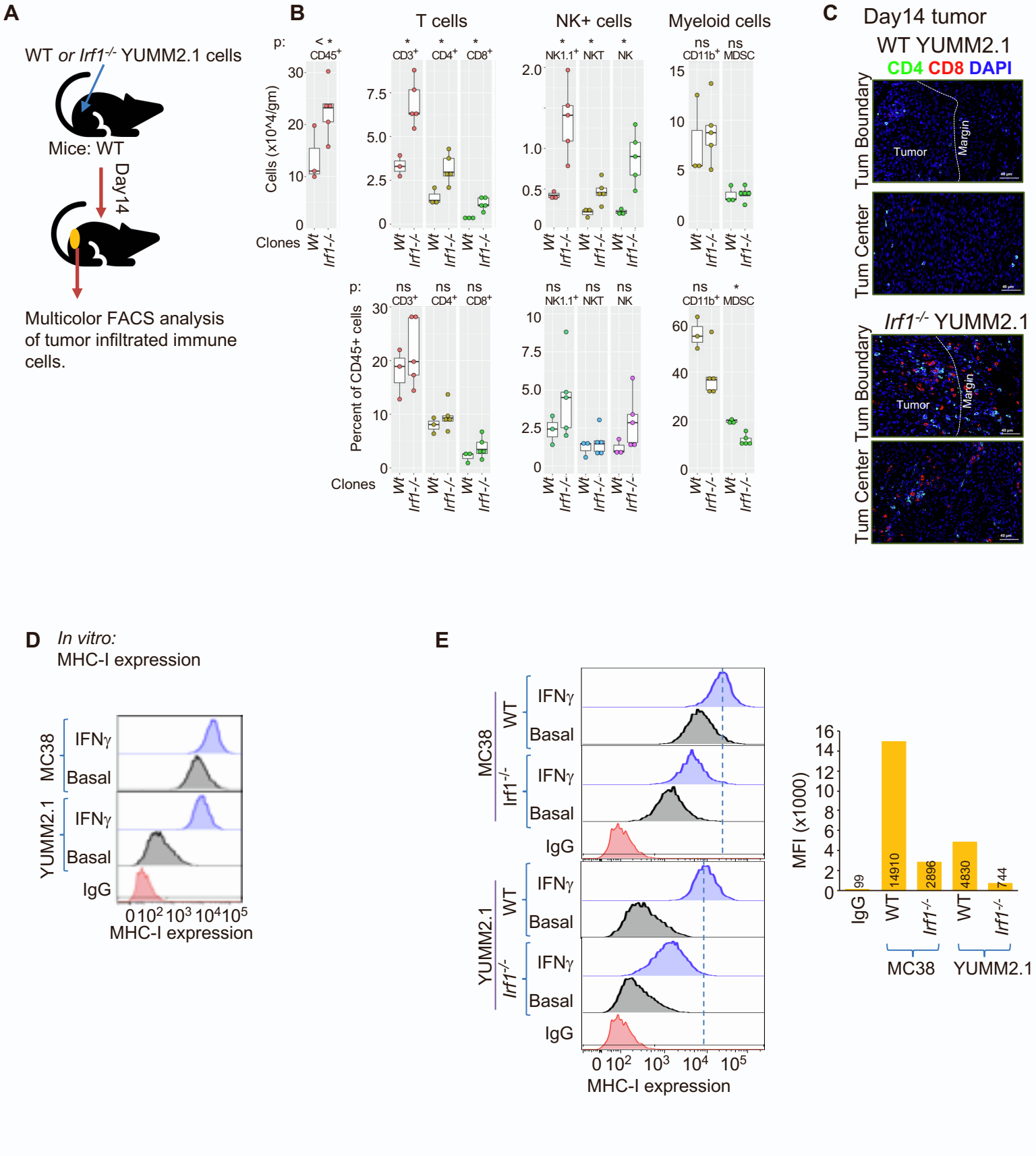

Figure S2. Increased Infiltration of Innate Lymphoid Cells is Associated with Growth Impairment of Poorly Immunogenic *Irf1*$^{-/-}$ Tumor. (**A)** Schematic representation of syngeneic tumor model; WT *and Irf1*$^{-/-}$ YUMM2.1 tumor cells were used to subcutaneously inject into WT mice and tumor growth was monitored as depicted. **(B)** Highlights the greater infiltration of NK cells relative to CD4^{+}, CD8^{+} and NKT cells in the *Irf1*$^{-/-}$ YUMM2.1 tumors from WT mice. Upper and lower panels represent indicated immune cells "per gram of tumors" and "percentage of CD45^{+} cells" respectively. **(C)** Immunofluorescence staining of YUMM2.1 tumors showing increased infiltration of CD8^{+} and CD4^{+} cells at the tumor-center and tumor-microenvironment boundary. **(D)** Shows low level of surface MHC-I expression in YUMM2.1 as compared to MC38, which is induced by IFN-γ (100 units/ml, 18h). **(E)** Left histograms show surface expression of MHC-I at baseline and after stimulation with IFN-γ (100 units/ml for 18h) in WT and *Irf1*$^{-/-}$ tumor cell clones (MC38 and YUMM2.1). Right bar graph represents the average expression of MHC-I (MFI) in WT and *Irf1*$^{-/-}$ tumor cells to highlight diminished level of MHC-I expression in the *Irf1*$^{-/-}$ YUMM2.1 cell as compared to MC38. For B, P values were determined by a Mann-Whitney U/ Wilcoxon rank-sum test. * for $P \leq 0.05$; ** for $P < 0.01$; *** for $P < 0.001$; **** for $P < 0.0001$.

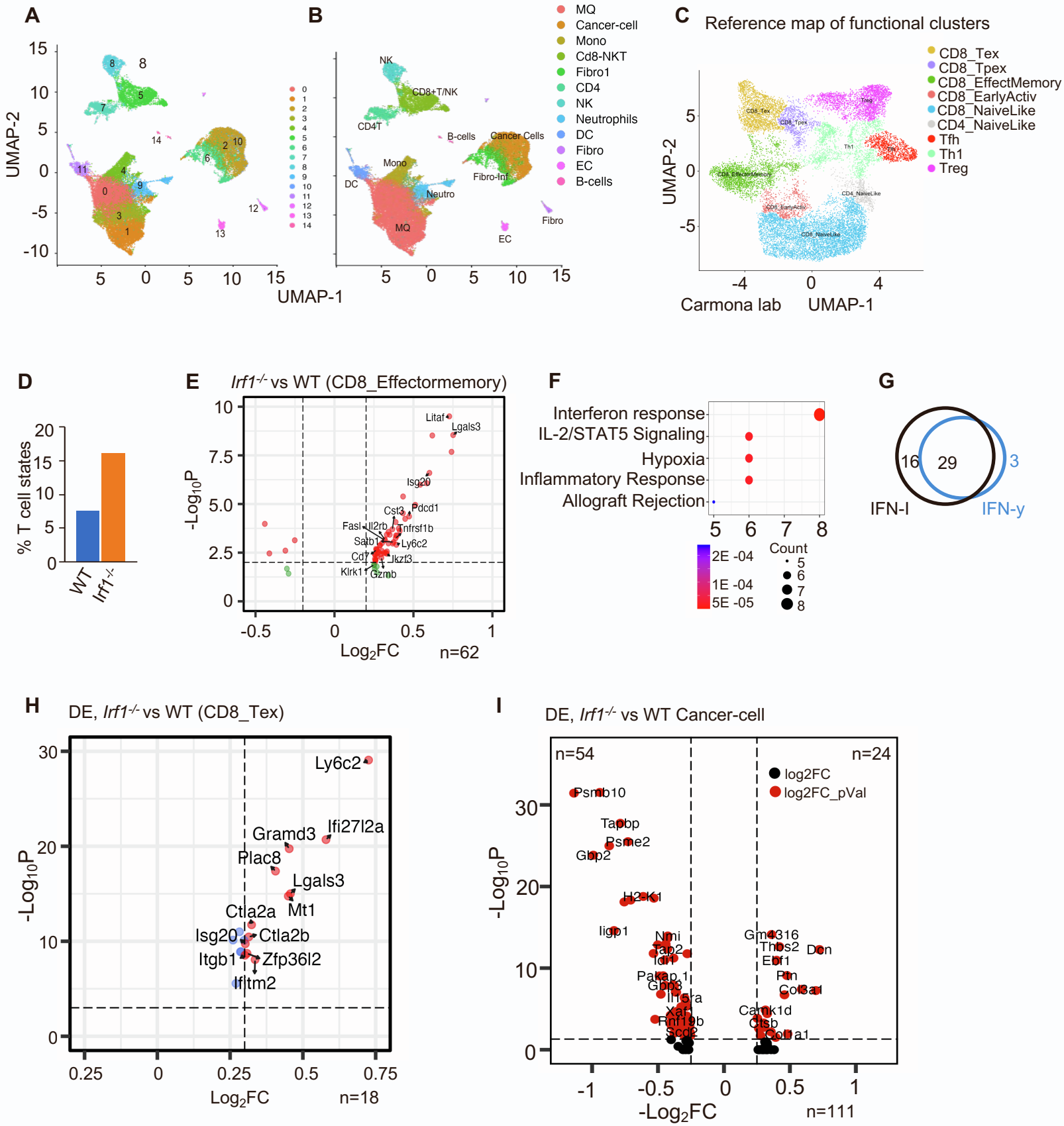
A
B
C
Reference map of functional clusters
MQ
Cancer-cell
Mono
Cd8-NKT
Fibro1
CD4
NK
Neutrophils
DC
Fibro
EC
B-cells
CD8_Tex
CD8_Tpex
CD8_EffectMemory
CD8_EarlyActiv
CD8_NaiveLike
CD4_NaiveLike
Tfh
Th1
Treg
UMAP-1
UMAP-2
Carmona lab
D
% T cell states
WT
Irf1-/-
E
Irf1-/- vs WT (CD8_Effectormemory)
-Log10P
Log2FC
n=62
F
Interferon response
IL-2/STAT5 Signaling
Hypoxia
Inflammatory Response
Allograft Rejection
Count
G
IFN-I
IFN-γ
16
29
3
H
DE, Irf1-/- vs WT (CD8_Tex)
Log2FC
n=18
I
DE, Irf1-/- vs WT Cancer-cell
n=54
n=24
log2FC
log2FC_pVal
-Log2FC
n=111
J
GO, upregulated genes in Cancer-cells
Extracellular matrix organization
Extracellular structure organization
External encapsulating structure organization
Peptide cross-linking
Collagen metabolic process
Count
p.adj
Dcn,Postn,Col3a1,Col1a1, Ptn, Brinp3, Thbs2, Ebf1, Serpinf1, Bgn, Gm4316, Tnc, Fn1, Afp, Col5a2, Mmp14, Acta2, Ccl7, Col5a1, Ifi27l2a,Camk1d, Mki67, Palld, Ctsb
GO, down regulated genes in Cancer-cells
Interferon- beta response
Antigen processing and presentation
Cellular response to IFN-β
Cellular response to IFN-γ
Psmb8,Gbp2,Psmb10,Fdps,Iigp1,Tapbp,Zbp1,Psme2,Psmb9, H2-K1, Irf1,Psme1, Cxcl10, Msmo1, Hmgcs1, Gbp7,Pakap.1,Idi1, Gbp3, H2-D1, Tap2, Insl6,Nmi,H2-Q7, Igtp, Egr1, Neat1, Ifi47,Idnk, Plaat3, Gm16685, Irgm1, Apobec3,Nfkbia, H2-T22, Cyp51, Fos, Mast4, Xaf1, Tap1, Rnf19b, Gm4951, Sox9,Rhob,Jun, Scd2, Ttc39c,Ier5, Oasl2,Klf2,Utrn, Fads2,Tnnt2,Parp14

Figure S3. (Related to Figure 3) (A) UMAP showing 15 distinct conserved clusters of cells identified by integrated Seurat analysis of scRNA-seq of WT and *Irf1*$^{-/-}$ MC38 tumors. **(B)** Based on the expression of cell type specific marker genes, these 15 clusters are reduced to indicated 12 cell types. **(C)** A reference T cell atlas from ProjectTILs showing 9 distinct T cell states that is used as reference to project sc-RNA-seq data from WT and *Irf1*$^{-/-}$ tumors in Fig 2D. **(D)** More than double proportion of T cells are mapped to reference from *Irf1*$^{-/-}$ tumors as compared to that of the WT tumors. **(E)** Differentially expressed (DE) genes in CD8_effectormemory cells, reveals induced expression of ISGs in cells from *Irf1*$^{-/-}$ tumors. **(F)** Gene ontology analysis MSigDB Hallmark 2020 gene sets in Enrichr indicates that interferon and IL2/ STAT5 signaling pathway genes are over expressed in CD8_effectormemory like cells from *Irf1*$^{-/-}$ as compared to WT tumors. **(G)** Interferome data base (http://www.interferome.org) indicated 48 out of 56 genes that are over expressed in CD8_effectormemory like cells from *Irf1*$^{-/-}$ tumors are ISGs and majority of type-I IFN inducible (45 out of 48) as compared to IFN-γ inducible (32 out of 48). **(H)** DE genes in CD8_Tex cells indicating elevated expression of the ISGs (*Isg20*, *Ifitm2*) and T cell activation marker genes (*Ly6C2*). **(I)** Volcano plot showing reduced expression of some of the ISGs in differentially expressed genes between *Irf1*$^{-/-}$ and WT cancer cell clusters. **(J)** Bar graph, left panel shows overrepresented pathways in genes that are upregulated in *Irf1*$^{-/-}$ cancer cells cluster. right panel shows pathways overrepresented in genes that are down regulated in *Irf1*$^{-/-}$ cancer cells cluster, which includes interferon response pathways.

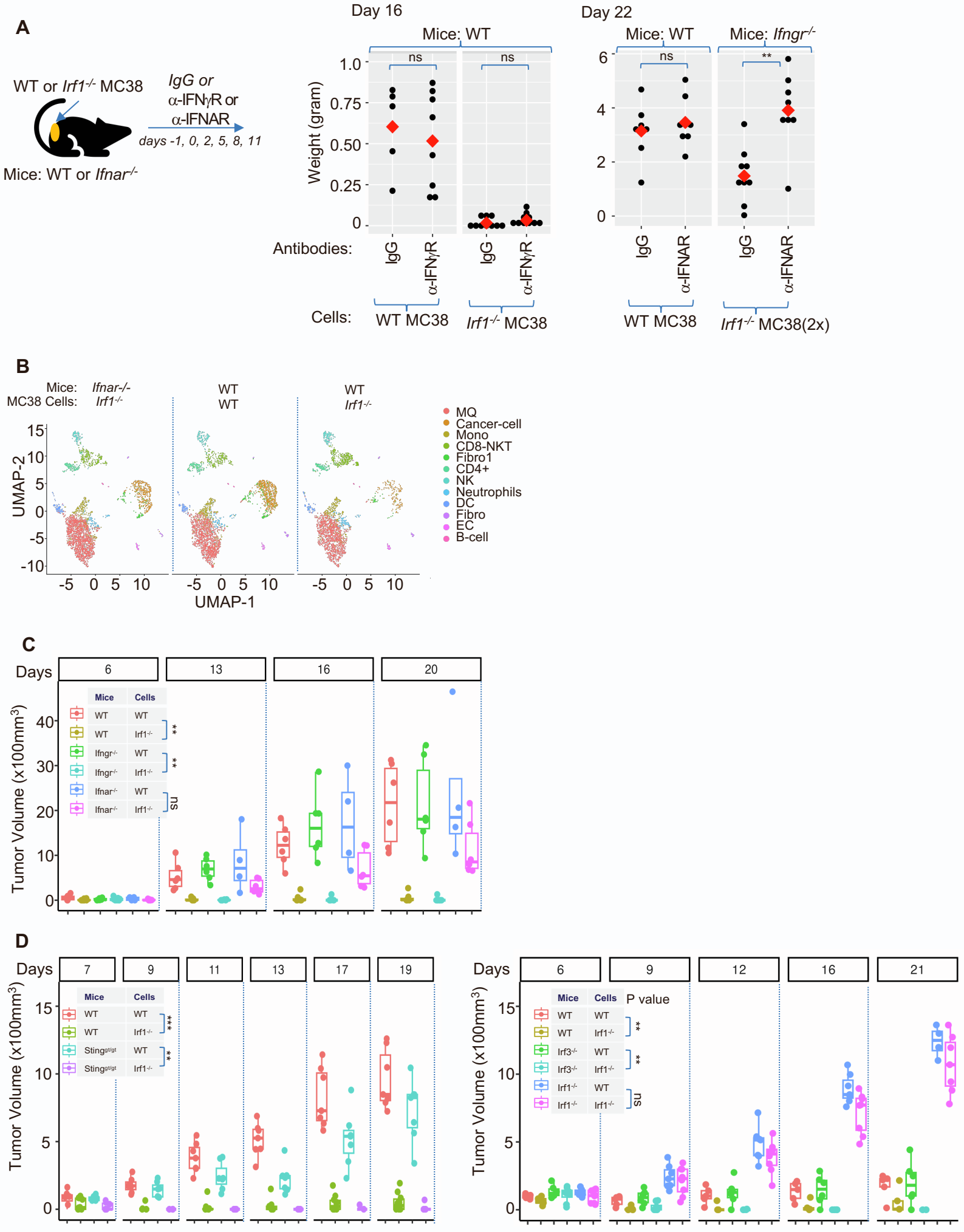
A
WT or Irf1-/- MC38
IgG or
α-IFNγR or
α-IFNAR
days -1, 0, 2, 5, 8, 11
Mice: WT or Ifnar-/-
Day 16
Mice: WT
Weight (gram)
ns
ns
Antibodies:
IgG
α-IFNγR
IgG
α-IFNγR
Cells:
WT MC38
Irf1-/- MC38
Day 22
Mice: WT
Mice: Ifngr-/-
ns
**
IgG
α-IFNAR
IgG
α-IFNAR
WT MC38
Irf1-/- MC38(2x)
B
Mice: Ifnar-/-
MC38 Cells: Irf1-/-
WT
WT
WT
Irf1-/-
UMAP-2
UMAP-1
MQ
Cancer-cell
Mono
CD8-NKT
Fibro1
CD4+
NK
Neutrophils
DC
Fibro
EC
B-cell
C
Days
6
13
16
20
Mice
Cells
WT
WT
WT
Irf1-/-
Ifngr-/-
WT
Ifngr-/-
Irf1-/-
Ifnar-/-
WT
Ifnar-/-
Irf1-/-
**
**
ns
Tumor Volume (x100mm3)
D
Days
7
9
11
13
17
19
Mice
Cells
WT
WT
WT
Irf1-/-
Stinggt/gt
WT
Stinggt/gt
Irf1-/-
***
**
Tumor Volume (x100mm3)
Days
6
9
12
16
21
Mice
Cells
P value
WT
WT
WT
Irf1-/-
Irf3-/-
WT
Irf3-/-
Irf1-/-
Irf1-/-
WT
Irf1-/-
Irf1-/-
**
**
ns
Tumor Volume (x100mm3)

Figure S4. (Related to Figure 4) Host's IFN-I Signaling Primarily Suppresses *Irf1*$^{-/-}$ Tumor Growth and Contributes to Effector T Cell Like Population in the *Irf1*$^{-/-}$ Tumors. (A) Schematic representation of strategies to test the roles of type I IFN and IFNy in the control of WT and *Irf1*$^{-/-}$ tumors. Middle dot plot shows that blockade of IFNGR does not impact WT and *Irf1*$^{-/-}$ tumors. Right dot plot represents that blockade of IFNAR greatly enhance the *Irf1*$^{-/-}$ tumor growth in *Ifngr*$^{-/-}$ mice. **(B)** Uniform Manifold Approximation and Projection (UMAP) of single cell RNA-seq data from "*Irf1*$^{-/-}$ MC38 tumors grown in *Ifnar*$^{-/-}$ mice", "WT MC38 tumors grown in WT mice" and "*Irf1*$^{-/-}$ MC38 tumors grown in WT mice", related to Fig 4B. **(C)** Related to Figure 4A, dot plot represents volume of WT and *Irf1*$^{-/-}$ MC38 tumors in WT, *Ifngr*$^{-/-}$, and *Ifnar*$^{-/-}$ mice on on indicated days post cell injection (**D)** Related to Figure 4G, Middle plot shows volume of WT and *Irf1*$^{-/-}$ MC38 tumor in WT and *Sting*$^{gt/gt}$ mice and right plot shows volume of WT and *Irf1*$^{-/-}$ tumors in the WT, *Irf3*$^{-/-}$ and *Irf1*$^{-/-}$ mice on indicated days post cells injection. For plots in A, C and D, P values were determined by a Mann-Whitney U/ Wilcoxon rank-sum test. * for $P \leq 0.05$; ** for $P < 0.01$; *** for $P < 0.001$; **** for $P < 0.0001$.

A Tumor infiltrating T cells populations (WT vs *Irf1*$^{-/-}$ mice)

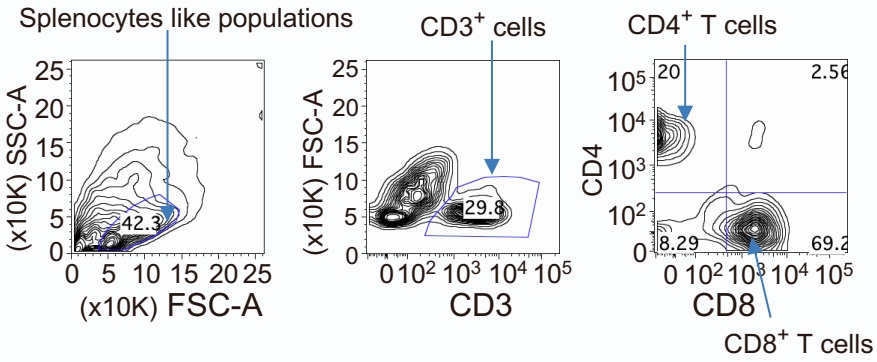

B Tumor infiltrating NK and NKT cells populations (WT vs *Irf1*$^{-/-}$ mice)

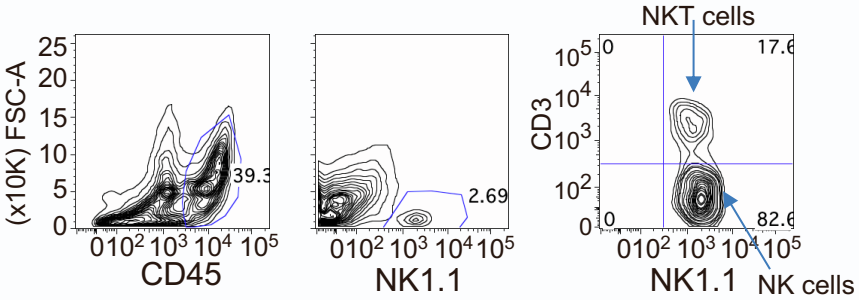

C

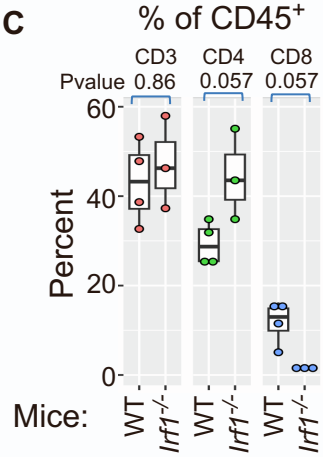

D

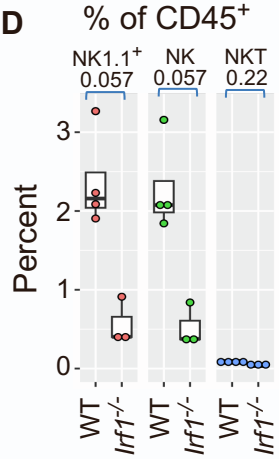

Figure S5 (Related to Figure 5). Gating scheme to profile tumor infiltrated T cell sub populations **(A),** and NK and NKT cells populations **(B)**. **(C)** Frequency of total T "$CD3^{+"}$, helper T "$CD4^{+}$" and cytotoxic T "$CD8^{+}$" cells relative to $CD45^{+}$ cells in the spleen of WT (n=4) and *Irf1*$^{-/-}$ mice (n=3). Mean frequencies for CD3, $CD4^{+}$ T and $CD8^{+}$ T cells in WT spleen are 43.2 %, 29.36% and 11.8%, respectively. Mean frequencies for CD3, $CD4^{+}$ T and $CD8^{+}$ T cells in *Irf1*$^{-/-}$ spleen are 47.1 %, 44.5% and 1.6%, respectively. **(D)** Frequency of "total NK1.1", "NK" and "NKT" cells relative to $CD45^{+}$ cells in the spleen of WT (n=4) *and Irf1*$^{-/-}$ (n=3) mice. Mean frequencies of NK1.1+, NK and NKT cells in WT spleen are 2.4 %, 0.084% and 2.28%, respectively. Mean frequencies of NK1.1+, NK and NKT cells in *Irf1*$^{-/-}$ spleen are 0.6 %, 0.043% and 0.52%, respectively.

A

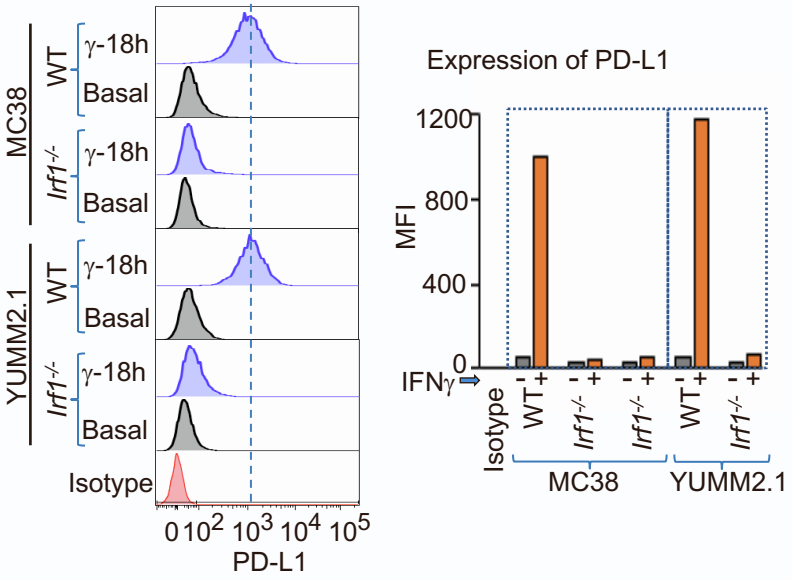

B

Basal gene expression change *Irf1*$^{-/-}$ cells

RPKM>1; FC=3, P<0.05, n=71

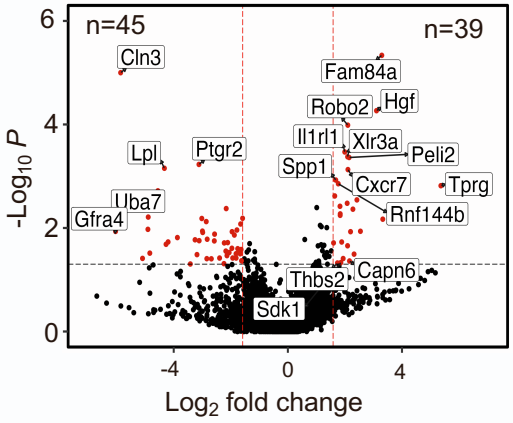

C GO term for Basal downregulated genes in IRF1KO

Term	P-value	Genes
MHC1 Causes Antigen Presentation Failure in Cancer Immune Escape	2.73E-07	TAP2;PSMB8;PSMB9;TAPBP
Proteins with Altered Expression in Cancer Immune Escape	4.05E-06	TAP2;PSMB8;PSMB9;TAPBP
MHC1-Mediated Antigen Presentation	2.20E-04	TAP2;TAPBP
Genes with Mutations in Cancer Immune Escape	2.69E-04	TAP2;TAPBP
Endogenous Peptide Antigen Presentation	0.01342584	TAPBP
Estrogen Deficiency in Female Obesity	0.02007253	LPL
Familial Partial Lipodystrophy Type 3 Progression (Hypothesis)	0.02227835	LPL
Proteins with Altered Expression in Atopic Dermatitis	0.02447932	CDSN
IL15R -> NF-kB/NFATC Signaling	0.02447932	IL15RA
IL15R -> STAT Signaling	0.02447932	IL15RA

D GO term for Basal upregulated genes in IRF1KO

Term		P-value	Genes
Epithelial Mesenchymal Transition		2.30E-06	TGFBR3;COL3A1;LOX;MMP3;SPP1;THBS2
Angiogenesis		0.00223848	COL3A1;SPP1
Inflammatory Response		0.00690907	PTGER4;RNF144B;OSMR
UV Response Dn		0.03206304	TGFBR3;COL3A1
Apoptosis		0.0392922	TGFBR3;HGF
IL-2/STAT5 Signaling		0.05740551	IL1RL1;SPP1
Hypoxia		0.05791557	LOX;PPP1R3C
Myogenesis		0.05791557	COL3A1;PPP1R3C
IL-6/JAK/STAT3 Signaling		0.15648845	OSMR
Spermatogenesis		0.23232899	IL13RA2

E

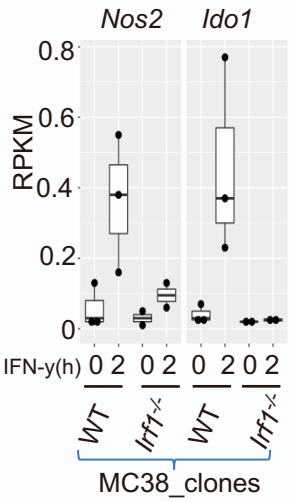

Figure S6. (Related to Figure 6) IFN-γ Inducible but not the Basal Expression of PD-L1 is Dependent on IRF1. (A) In left, histogram shows comparable basal expression of PD-L1 on MC38 and YUMM2.1 cell lines and also highlights absolute dependence of IFN-γ induced PD-L1 expression on IRF1 in MC38 as well as in YUMM2.1 cells. Right bar graph summarizes the MFI of PD-L1 expression in WT and *Irf1*$^{-/-}$ cell clones. **(B)** Volcano plot of all the expressed genes (at basal level) showing DE genes between WT and *Irf1*$^{-/-}$ MC38 cells. This identified 45 downregulated (top left quadrant) and 39 upregulated (top right quadrant) genes in *Irf1*$^{-/-}$ cells relative to WT cells. **(C)** Gene Ontology analysis of genes with reduced basal expression in *Irf1*$^{-/-}$ cells reveals enrichment of pathways required for MHC-I mediated antigen presentation. **(D)** Gene Ontology analysis of genes with enhanced basal expression in *Irf1*$^{-/-}$ cells, which are overrepresented in epithelial to mesenchymal transition pathway. **(E)** RPKM expression of *Nos2* and *Ido1* in WT and *Irf1*$^{-/-}$ cells, which shows strong dependence of both genes on IRF1 during IFN-γ signaling.

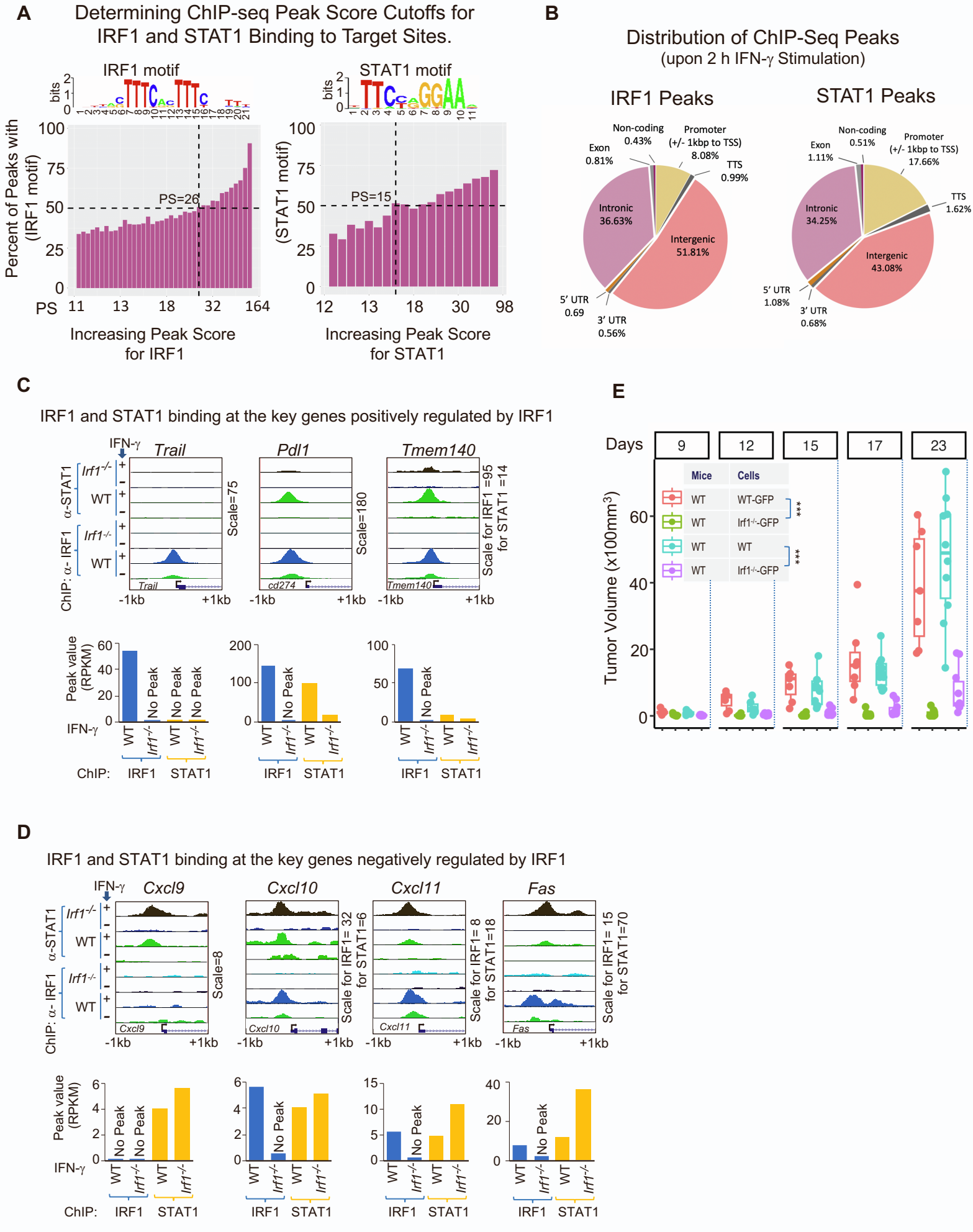
A
Determining ChIP-seq Peak Score Cutoffs for IRF1 and STAT1 Binding to Target Sites.
IRF1 motif
STAT1 motif
bits
Percent of Peaks with (IRF1 motif)
(STAT1 motif)
PS=26
PS=15
PS 11 13 18 32 164
12 13 18 30 98
Increasing Peak Score for IRF1
Increasing Peak Score for STAT1
B
Distribution of ChIP-Seq Peaks
(upon 2 h IFN-γ Stimulation)
IRF1 Peaks
STAT1 Peaks
Exon 0.81%
Non-coding 0.43%
Promoter (+/- 1kbp to TSS) 8.08%
TTS 0.99%
Intronic 36.63%
Intergenic 51.81%
5' UTR 0.69
3' UTR 0.56%
Exon 1.11%
Non-coding 0.51%
Promoter (+/- 1kbp to TSS) 17.66%
TTS 1.62%
Intronic 34.25%
Intergenic 43.08%
5' UTR 1.08%
3' UTR 0.68%
C
IRF1 and STAT1 binding at the key genes positively regulated by IRF1
IFN-γ
Trail
Pdl1
Tmem140
ChIP: α- IRF1 α-STAT1
Irf1-/-
WT
Scale=75
Scale=180
Scale for IRF1 =95 for STAT1 =14
-1kb +1kb
Peak value (RPKM)
No Peak
ChIP: IRF1 STAT1
D
IRF1 and STAT1 binding at the key genes negatively regulated by IRF1
Cxcl9
Cxcl10
Cxcl11
Fas
Scale=8
Scale for IRF1= 32 for STAT1=6
Scale for IRF1= 8 for STAT1=18
Scale for IRF1= 15 for STAT1=70
E
Days 9 12 15 17 23
Tumor Volume (x100mm3)
Mice Cells
WT WT-GFP
WT Irf1-/--GFP
WT WT
WT Irf1-/--GFP
***
***

Figure S7. (Related to Figure 7) Detailed Quantitative Analysis of ChIP-seq Peaks Reveals Distinct Mode of IRF1 and STAT1 Binding to Regulate their Target Genes Expression. (A) X-axis shows increasing ChIP-seq peak score separated into 38 (left panel) and 19 (right panel) bins for IRF1 and STAT1 called peaks respectively and Y axis shows percentage of peaks with consensus motifs. The dotted lines on plots shows selection of bins with 50% of their called peaks with a recognizable motif. **(B)** Pie charts showing distribution of IRF1 (left) and STAT1 (right) peaks in various genomic locations in IFN-γ stimulated cells. **(C)** Upper panel displays genome browser tracks for the binding of IRF1 and STAT1 within 1kb of the TSSs of genes positively regulated by IRF1, in unstimulated and IFN-γ stimulated, WT and *Irf1*$^{-/-}$ MC38 cells. Lower panel shows the quantitative values of the peaks shown in the upper panels. This highlights that IRF1 dictates expression of these genes as loss of its binding in *Irf1*$^{-/-}$ also diminishes STAT1 binding at the promoters where IRF1 co binds along with STAT1 (*Pdl1 and Tmem140*). **(D)** Upper panel displays genome browser tracks for the binding of IRF1 and STAT1 within 1kb of the TSSs of genes either not regulated or negatively regulated by IRF1, in unstimulated and IFN-γ stimulated, WT and *Irf1*$^{-/-}$ MC38 cells. Lower panel shows the quantitative values of the peaks shown in the upper panels. This highlights that in IFN-γ stimulated *Irf1*$^{-/-}$ cells, STAT1 binds comparably or strongly to the genes that are either independent or are influenced negatively by IRF1(*Cxcl9-11*, and *Fas*). **(E)** Related to Fig 7I, plot showing volume of tumors on indicated days in WT hosts that were injected with GFP or PD-L1 over-expressing WT and *Irf1*$^{-/-}$ MC38 cells. For E, P values were determined by a Mann-Whitney U/ Wilcoxon rank-sum test. * for $P \leq 0.05$; ** for $P < 0.01$; *** for $P < 0.001$; **** for $P < 0.0001$.